Energy Advances

Accepted Manuscript

This article can be cited before page numbers have been issued, to do this please use: P. Rajbhandari, B. Rijal, Z. Chen, A. Choudhary, H. Efstathiadis and T. Dhakal, *Energy Adv.*, 2025, DOI: 10.1039/D5YA00072F.

ROYAL SOCIETY OF CHEMISTRY

rsc.li/energy-advances

View Article Online
DOI: 10.1039/D5YA00072F

ARTICLE

Performance enhancement of inverted perovskite solar cells through lithium-ion diffusion from nickel oxide hole transport layer to the perovskite absorber

Pravakar P. Rajbhandari,[a,b] Bipin Rijal, [a,b] Zeying Chen,[a,c] Ankit Choudhary, [d] Haralabos Efstathiadis[d] and Tara P. Dhakal [a-c]

Received 00th January 20xx,
Accepted 00th January 20xx

DOI: 10.1039/x0xx000042640x

Inverted perovskite solar cells, known for their low temperature processability and reduced hysteresis, benefit from the use of nickel oxide (NiOx) as a hole transport material, which enhances stability. The doping of NiOx with lithium improves its electrical properties by creating Ni^{3+} sites through intrinsic doping with Ni vacancies. This study investigated the impact of Li doping on the optical and electrical properties of NiOx and evaluated the optimal doping concentration for solar cell performance. Additionally, the diffusion of small sized Li ions from the NiOx hole transport layer into the photoactive perovskite layer has been investigated, which lead to the improvement of the perovskite absorber quality through defect passivation caused by lithium diffusion from the NiOx layer, enhancing device performance. The incorporation of lithium significantly boosted all solar cell parameters, leading to a 60.8% increase in power conversion efficiency (PCE), from approximately 12% to a maximum of 19.3%.

Introduction

Perovskite based solar cells have witnessed tremendous growth in short period of time and efforts for their commercialization have been the top priority[1–3]. Even though conventional n-i-p (negative-intrinsic-positive) structured perovskite solar cells (PSCs) have achieved the highest performance thus far, there is a growing interest in inverted (p-i-n) planar device architecture due mainly to its relatively simple fabrication process and negligible hysteresis effect.[4–6] The basic p-i-n architecture consists of an intrinsic absorber sandwiched between the hole and electron transport layers (HTL and ETL). A wide range of HTLs, both organic and inorganic, have been studied to determine their suitability for use in inverted architecture solar cells. One of the most critical properties of HTL in inverted structure devices is that its bandgap must be wide enough to allow more light to reach the perovskite absorber layer. Second, the HTL should effectively block electrons from moving toward the front transparent electrode such as indium tin oxide (ITO). Inorganic materials such as Nickel oxide (NiOx) are of particular interest due to their low cost, higher carrier mobility, and chemical stability.[9,10] These inorganic HTLs are not only stable in the presence of the ITO layer beneath them but are also not affected by the following synthesis processes.[11] The cubic p-type semiconductor NiOx is one of the most promising materials for HTL in perovskite solar cells, which has several advantages over the other counterparts, such as high transmittance in visible spectral range, and good tolerance to chemical and thermal treatments.[9,12–15] Beyond that, NiOx has a good band alignment with most of the perovskite absorbers due to its wide band gap (3.5-4.0eV) and high work function.[16–18]

However, the poor conductivity (2.67 x 10^{-6} S cm^{-1}) of NiOx limits the hole extraction efficiency, which results in a high series resistance, that adversely affects the current density (J_{SC}) and fill factor (FF) of the perovskite solar cells.[10] Moreover, the low conductivity also causes a hole accumulation at the interface with perovskite, which leads to increased interfacial recombination and reduced charge transport.[15] The stoichiometric NiOx (x=1) with Ni^{2+} oxidation state insulates the charge carriers. The commonly observed p-type conductivity in undoped NiOx is due to the presence of Ni^{2+} vacancy. However, the ionization energy of Ni^{2+} vacancy is significant, /which limits the hole density and conductivity of p-type NiOx.[10,19] The NiOx conductivity can be considerably improved by increasing the concentration of Ni^{3+} ions by introducing the nickel vacancies and the interstitial oxygen atoms in the NiOx crystals.[20] Depending on the fabrication process, the stoichiometry and the corresponding conductivity can be changed. Doping with extrinsic elements with shallower acceptor levels has been the most effective method to enhance the conductivity and adjust work function as well as band alignment of NiOx with perovskite to minimize losses.[10,18] A deeper work function with a Fermi

[a] Center for Autonomous Solar Power (CASP), Binghamton University, Binghamton, NY 13902, USA
[b] Department of Electrical and Computer Engineering, Binghamton University, Binghamton, NY 13902, USA
[c] Materials Science and Engineering Program, Binghamton University, Binghamton, NY 13902, USA
[d] Department of Nanoscale Science & Engineering, University at Albany, State University of New York, Albany, NY 12222, USA

Supplementary Information available: [details of any supplementary information available should be included here]. See DOI: 10.1039/x0xx00000x

View Article Online DOI: 10.1039/D5YA00275F

level around the midgap can enhance the open-circuit voltage (V_{OC}) of solar cells.

A variety of dopants have been investigated to improve the conductivity of NiOx that include Li^+,[9] Cs^+,[21] La^{3+},[22] Cu^{2+},[23] Zn^{2+},[24] Al^{3+},[25] Co^{2+},[26] Ce^{4+},[10] self-dopant Ni^{3+},[27] molecular dopant 2,2'-(per- fluoronaphthalene-2,6-diylidene) dimalononitrile (F6TCNNQ),[28] and co-dopant, such as Li^+:Cu^{2+},[15] Li^+:Mg^{2+},[29] Ce:Zn^{2+}.[30] Monovalent alkali metal lithium (Li) can effectively p-type dope NiOx, which improves the electrical conductivity without significantly affecting the light-transmitting performance of the NiOx films. Li^+ (Li-ion) (0.72-0.76 Å) has a similar ionic radius to Ni^{2+} (0.69-0.74 Å), which minimizes the doping mismatch and enhances the lattice stability as well.[32] Various techniques, such as spin coating,[33] spray pyrolysis,[11,34] pulsed laser deposition (PLD),[35] sputtering,[36,37] etc., have been used to fabricate Li-doped NiOx. Li has a relatively shallower acceptor level in NiOx for Ni-poor/O-rich conditions.[38] The doping is achieved through Ni^{2+} substitutional replacement with Li-ion, which leads to an increase in Ni^{3+} density and improves the electrical conductivity of NiOx thin film.[20,39] Doping NiOx with Li lowers the ionization energy of the Ni vacancies and thereafter improves the hole conductivity in NiOx films. The resistivity of NiOx has been reported to be in the range of 10–10^6 Ω cm.[40] A dramatic decrease in resistivity, down to 0.15 Ω cm, was achieved by increasing Li-ion concentration up to 7% because Li-ion goes into Ni^{2+} substitutional sites, which in turn increases hole density and enhances the p-type conductivity.[41] Li-doped NiOx was also discovered to dramatically suppress trap-assisted recombination at interfacial contact compared with PEDOT:PSS due to the improved crystallinity of perovskite grown on Li-doped NiOx and superior perovskite/NiOx interface.[47] Zhao et al. reported the use of Li:NiO/NiO bilayer to improve carrier extraction, transport, and radiative recombination at NiO/perovskite interface.[18] It was demonstrated that by tuning Li doping amount, the Ni^{3+} ratio in NiOx film and interfacial oxidation could be controlled, which results in improved photovoltaic performance by incorporating the $Ni^{3+} \leftrightarrow Ni^{2+}$ ion pairs as the interfacial passivation species.[32] While the incorporation of alkali metal cations as additives to the perovskite layer has brought a significant reduction in defect density of the perovskite, the migration of Li-ions from hole transport layer to the perovskite absorber layer has also been reported to suppress the defects formation and hysteresis, thereby enhancing the performance of perovskite solar cells.[48] The migrated Li-ions that reside at grain boundaries of perovskite crystals were found to attract the photogenerated electrons and repel the holes, which thereby reduced the probability of recombination at those grain boundaries[49].

Motivated by the above studies, we examined the doping of nickel oxide with Li and demonstrated its impact on the electrical and optical properties of the material. The NiOx was doped with various amounts of Li, which was then used as an HTL in the fabrication of the PSCs. The inclusion of Li-ions in the NiOx HTL in our inverted perovskite solar cell configuration served a dual purpose: firstly, it enhanced the conductivity of NiOx by making it more p-type; and secondly, the diffusion of Li ions to the perovskite absorber layer passivated the defect states, which thereby reduced the non-radiative recombination. Although the migration of Li-ion from charge transport layer to subsequent perovskite layer has been reported for regular (nip) structured PSCs, this is the first time we have observed such phenomena in inverted (pin) structured PSCs. This led to significant improvement in the power conversion efficiencies of our solar cells from 12% to more than 19% upon optimal (8% concentration) Li doping, which originated from the significant improvements of short-circuit photocurrent (J_{sc}) and fill factor (FF). This work confirmed that Li-doped NiOx is a promising hole transport material (HTM) for high-performance inverted PSCs.

Experimental

Materials and methods: ITO-coated plain glass substrates were cleaned by sonicating in acetone and isopropyl alcohol. Subsequently, the substrates were subjected to a UV-ozone treatment for 15 min. The fabrication of NiOx film was achieved by spin-coating 0.5 M nickel nitrate hexahydrate (Sigma-Aldrich, ≥97%) and ethylenediamine (Alfa Aesar, 99%) in ethylene glycol (Fisher, 99%) on ITO substrates. The doped-NiOx was composed of a controlled percentage of lithium nitrate (Alfa Aesar, 99%) into the 0.5 M solution. The spin-coated films were annealed at 300°C in air for 1 hr. After annealing, the NiOx-coated substrates were moved into the glovebox for further processing. Cesium containing triple cation perovskite ($CsFAMAPb(IBrCl)_3$) was fabricated with a two-step spin-coating process. Further details on perovskite synthesis can be found in our previous study.[50] Then, the perovskite films were annealed at 140°C for 20 min. After cooling down, 17 mg/ml [6,6]-Phenyl C61 butyric acid methyl ester (PCBM, Nano-C) in chlorobenzene (Sigma-Aldrich, 99%) was spin coated at 2000 rpm for 40 sec. and post-baked at 70°C for 2 min. An additional buffer layer of ZnO(4 nm)/Al_2O_3(1 nm) was deposited using Atomic Layer Deposition (ALD) at 100°C. More details on ALD process can be found in our previous report [51]. The samples were then taken to the thermal evaporator outside the glovebox to deposit 100 nm of silver.

Characterizations: The structural characterization of perovskite was performed with x-ray diffraction (XRD) on a PanAnalytical X'Pert PRO X-ray diffraction system, which uses CuKα X-rays and line-focus optics. Carl Zeiss supra 55 VP-high resolution-scanning electron microscope (HR-SEM) was used to study the morphology of the films. The photoluminescence (PL) was measured using Horiba's PL measurement system with a 532 nm laser and photomultiplier tube (PMT) detector. Transmittance was measured using the Ångstrom Sun Technologies' TF Probe UV/Vis spectrophotometer. Time of flight secondary ion mass spectroscopy (TOF_SIMS) analysis was carried out using IONTOF Time of Flight SIMS (TOF-SIMS) spectrometer. Details on TOF-SIMS measurement's experimental procedure can be found in supporting information. IV measurements were carried out using Keithley's 4200-SCS semiconductor characterization system along with the solar simulator from Photo Emission Tech. Cells were tested

under AM1.5G 100 mW/cm^2 illumination with the voltage swept in the forward and/or reverse directions with a scan rate of 0.4 V/s. External quantum efficiency (EQE) measurement was performed using the EQE system from PV measurements inc. XPS study was performed using a Surface Science Instruments SSX-100 with operating pressure ~2x10^{-9} Torr. Monochromatic Al Kα x rays (1486.6 eV) with 1 mm diameter beam size were used. Photoelectrons were collected at a 55° emission angle. A hemispherical analyzer determined electron kinetic energy using a pass energy of 150 V for wide/survey scans and 50 V for high-resolution scans. A flood gun was used for charge neutralization of non-conductive samples. The band structure of the film was measured using ultraviolet photoelectron spectroscopy (UPS) with He-I as the excitation source. The UPS samples were prepared on ITO substrates.

Results and discussion

Study of the NiOx hole transport layer: The deposition of the undoped NiOx film was first optimized. We initially determined the optimal annealing temperature for the NiOx layer to be 300^{o}C by comparing the optical transmission of NiOx films annealed at various temperatures (Figure S1). Subsequently, the thickness of the NiOx film was controlled by adjusting the concentration of the precursor solution, which consisted of nickel nitrate hexahydrate and ethylenediamine dissolved in ethylene glycol, and the spin speed. To further investigate the impact of HTL thickness on device performance, we fabricated complete solar cell devices incorporating NiOx layers with varying thicknesses. The device configuration is shown in Figure 1a, where the perovskite layer is deposited using a two-step spin-coating method, following the optimized procedures established in our previous study.[52] The obtained NiOx film thicknesses and their corresponding device performances are presented in the supporting information (Figure S2-S4). Based on this experiment, an optimal and reproducible NiOx film thickness of around 25 nm was achieved with a precursor concentration of 0.5 M and a spin speed of 5500 rpm.

We then applied the optimized fabrication approach described above to investigate the effect of Li doping on NiOx. The NiOx shows a nanocrystalline structure, which is confirmed by top-view scanning electron microscopy (SEM) and atomic force microscopy (AFM) images in Figure S5-S6. Figure 1b shows the XRD pattern for undoped and (2-10) % lithium doped NiOx films. Three distinct peaks at 2θ equal to 37.3^o, 43.3^o and 63.2^o correspond to (111), (002) and (022) planes of cubic phase NiOx. The analysis also revealed that the incorporation of lithium did not alter the crystal structure of NiOx. The ionic radii of Li^+ (0.68 Å) and Ni^{2+} (0.69 Å) are similar, which explains the unaltered crystal structure of NiOx upon lithium doping[53]. The optical transmission of both doped (2%-10%) and undoped NiOx films deposited on glass exhibited high transmittance in the visible spectral range, with an average transmittance exceeding 90% (Figure 1c). As the Li doping concentration increased to 8%, the transmittance of the film slightly decreased, however at 10% doping, the transmittance decreased significantly. The higher Li content might have introduced scattering effect in the NiOx layer which caused the reduction in the transmittance.[54] The transmittance of the films was used to determine the bandgap of both Li-doped and undoped NiOx using Tauc plot method. The Tauc plot analysis did not show a significant change in optical bandgap (Figure 1d). When the doping concentration increased from 0% to 10%, the bandgap slightly red-shifted from 3.7 eV to 3.67 eV. This result is consistent with a previous study which reported that on the addition of 5% Li, the bandgap decreased from 3.6 eV (undoped NiOx) to 3.47 eV.[11] The high transmittance and bandgap of NiOx remained largely unaffected by Li doping up to a concentration of 8%.

The resistances of the undoped and (2% to 10%) Li-doped NiOx were measured using current voltage (I-V) characterization of the respective NiOx films sandwiched between ITO and high work function gold electrodes. The results revealed a decrease in resistance with an increase in Li-doping up to 4%, after which the resistance remained relatively stable until 8%. A slight increase in resistance was observed at 10% Li-doping level (Figure S7). This result shows the enhanced electrical conductivity of our NiOx HTL upon Li-doping. X-ray photoelectron spectroscopy (XPS) analysis revealed that the 8%

View Article Online
DOI: 10.1039/D5YA00072F

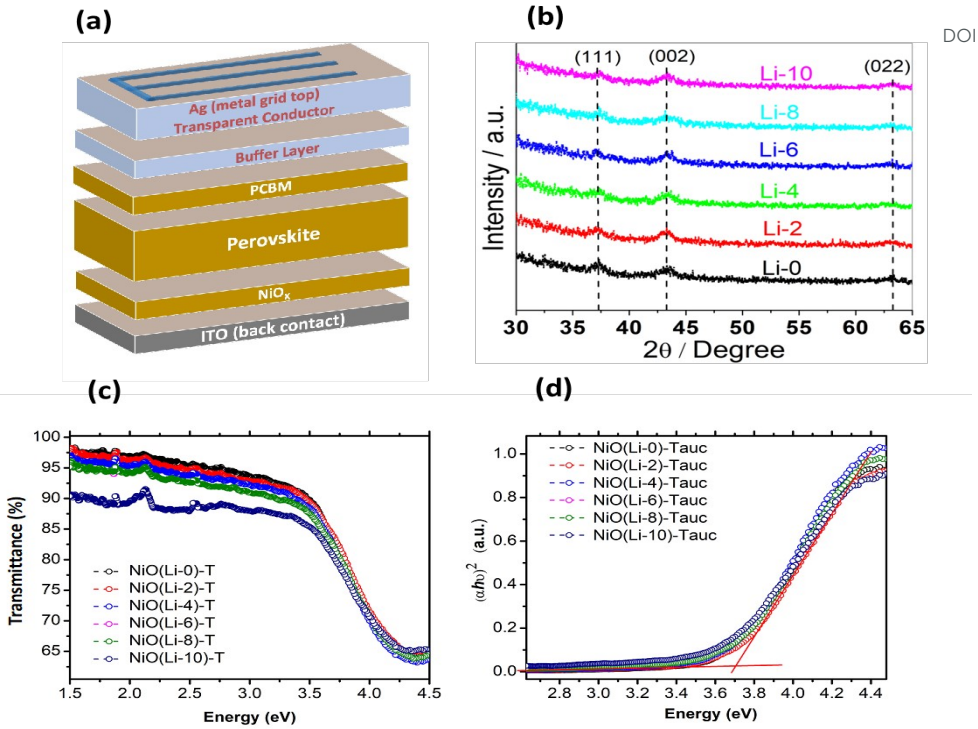

Figure 1 (a) Device structure for the solar cell, (b) XRD plots of different Li-doped NiOx films (c) Transmittance of different Li doped NiOx films, (d) Tauc plot for different Li-doped NiOx films.

Li-doped NiOx sample exhibited a higher concentration of Ni^{3+} states compared to the undoped sample (figure S8). This increase in the Ni^{3+} states contributed to the enhanced p-type behavior of the 8% Li doped NiOx layer, thereby improving its electrical conductivity relative to undoped NiOx layer.

Study of the Perovskite absorber layer: The crystallographic structure of perovskite layer grown on Li-doped NiOx with various Li concentrations was studied using Grazing Incidence X-ray Diffraction (GIXRD) analysis and the XRD patterns for the perovskite layer are revealed in Figure 2a. The results clearly demonstrated the identical diffraction peaks, indicating that the Li doping in the NiOx layer does not impact the formation of black-phase perovskite. The major peaks at 14.04°, 19.94°, 24.52°, and 28.3° are respectively assigned to (100), (110), (111), and (200) crystallographic planes of the perovskite.[55] The intensity of the major peaks at the (100) and (200) positions increased with higher Li doping in NiO_x, accompanied by a reduction in their full width at half maximum (FWHM). This enhancement reached its maximum at 8% Li doping, where the peaks exhibited the sharpest profiles. These results indicate the improved crystallinity of the perovskite film on 8% Li-doped NiO_X. To investigate the enhanced crystallinity of perovskite film deposited on Li-doped NiOx, we measured the surface roughness of undoped and 8% Li-doped NiOx films spin coated on glass substrates using AFM imaging (Figure 2b, 2c). The rms surface roughness of 8% Li-doped NiOx was 2.92 nm which is slightly higher compared to that of undoped NiOx (2.44 nm). The increased roughness might have provided higher nucleation sites to the perovskite growth thereby leading to the enhanced crystallinity.[56]

The steady-state photoluminescence (PL) spectra of perovskite films grown on glass, undoped NiO_X and Li-doped NiO_X substrates are presented in Figure 2d. The perovskite film grown on the Li-doped NiO_X demonstrated a remarkable improvement in the PL characteristics over the perovskite films deposited on glass and undoped NiO_X films. The enhancement in the PL intensity was observed with the addition of Li in NiOx and attained a maximum at 8% Li doping in the NiOx. However, a decrease in PL intensity was observed at 10% Li. These results indicate that the presence of Li in NiO_X enhanced the radiative recombination in perovskite film, most likely by the diffusion of Li ions into the perovskite and passivation of traps by filling the trap states before photoexcitation. Additionally, a slight redshift in agreement with the transmittance spectra of figure 1 was observed as the amount of Li doping increased, which is attributed to the intercalation of Li into the perovskite structure.[57,58]

It is well known that the Li ion is the smallest ion after hydrogen. Li ions exhibit a high diffusion tendency. The ionic mobility of Li in the perovskite is expected to be higher than that of the intrinsic ions due to its smaller size. The migration of Li through perovskite materials has been demonstrated in $MAPbI_3$ perovskites, which could potentially function as anode materials in Li-ion batteries.[59] Studies have reported that ions from perovskites can move into the hole or electron transport layers, which thereby enhances carrier-extraction ability and reduces interface recombination, which will result in reduced hysteresis[60]. Also, the migration of Li ions to grain boundaries of

View Article Online
DOI: 10.1039/D5YA00072F

perovskite crystals have been identified to reduce the nonradiative recombination within the perovskite film.[61] In our case too, the Li ions migrated from Li-doped NiOx HTL into the perovskite, which thereby improved the properties of the absorber and offered better carrier generation and extraction.

We studied the depth profile of a 100 nm perovskite layer, deposited on both 4% Li-doped and undoped NiOx layers, using time-of-flight secondary ion mass spectrometry (TOF-SIMS). In the Li-doped sample, we observed a clear lithium diffusion towards the perovskite layer, in which a pronounced increase near the perovskite surface exists (Figure 2e). This sharp increase may have resulted either from the accumulation of Li ions on the perovskite surface due to their smaller size and volatility or due to the contamination during the measurement. In contrast, no lithium was detected in the depth profile for undoped sample (Figure 2f and Figure S9 in the Supplementary Information). Such diffusion of Li ions from the hole transporting layer to the active perovskite layer has indeed been reported.[49]

To further investigate the effect of lithium diffusion into the perovskite layer, we fabricated hole-only devices with the structure FTO/Li-doped NiOx/Perovskite/PTAA/Ag. These devices were designed to determine the defect density within the bulk perovskite material. Dark I-V measurements were carried out to determine the trap-filled-limit voltage (V_{TFL}), which was then used to determine the trap-state density within the perovskite material based on the equation (1), where n_t, ε, q, and L are the trap state density, permittivity of the perovskite, elementary charge (1.6×10^{-19} C) and the thickness of the perovskite layer (450 nm).[62]

$$n_t = \frac{2\,V_{TFL}\,\varepsilon}{q\,L^2} \qquad (1)$$

We employed capacitance measurement of the perovskite layer (figure S10 supplementary information) to determine the dielectric constant of the perovskite layer to be 45. Figure 3a shows the decreased V_{TFL} for the perovskite layer deposited on 8% Li-doped NiOx HTL compared to the one deposited on undoped NiOx, corresponding to the trap-densities of 1.03×10^{16} cm^{-3} and 1.72×10^{16} cm^{-3} respectively, which confirms the reduction in trap states after Li-doping. The V_{TFL} and n_t calculations for the perovskite layers deposited on all 2 to 10% Li-doped NiOx are shown in supplementary figure S11 and supplementary table ST1. The results demonstrate reduction in trap states for the perovskite layers deposited on all Li-doping concentrations. These results align with the enhancement in the PL intensity of perovskite films, as discussed earlier.

Ultra-violet Photoelectron Spectroscopy (UPS) was carried out to obtain energy band information and work functions (WFs) change of NiO_X films upon Li doping and their alignment with the perovskite energy bands. The band energy values for ZnO and PCBM were taken from the literature and incorporated

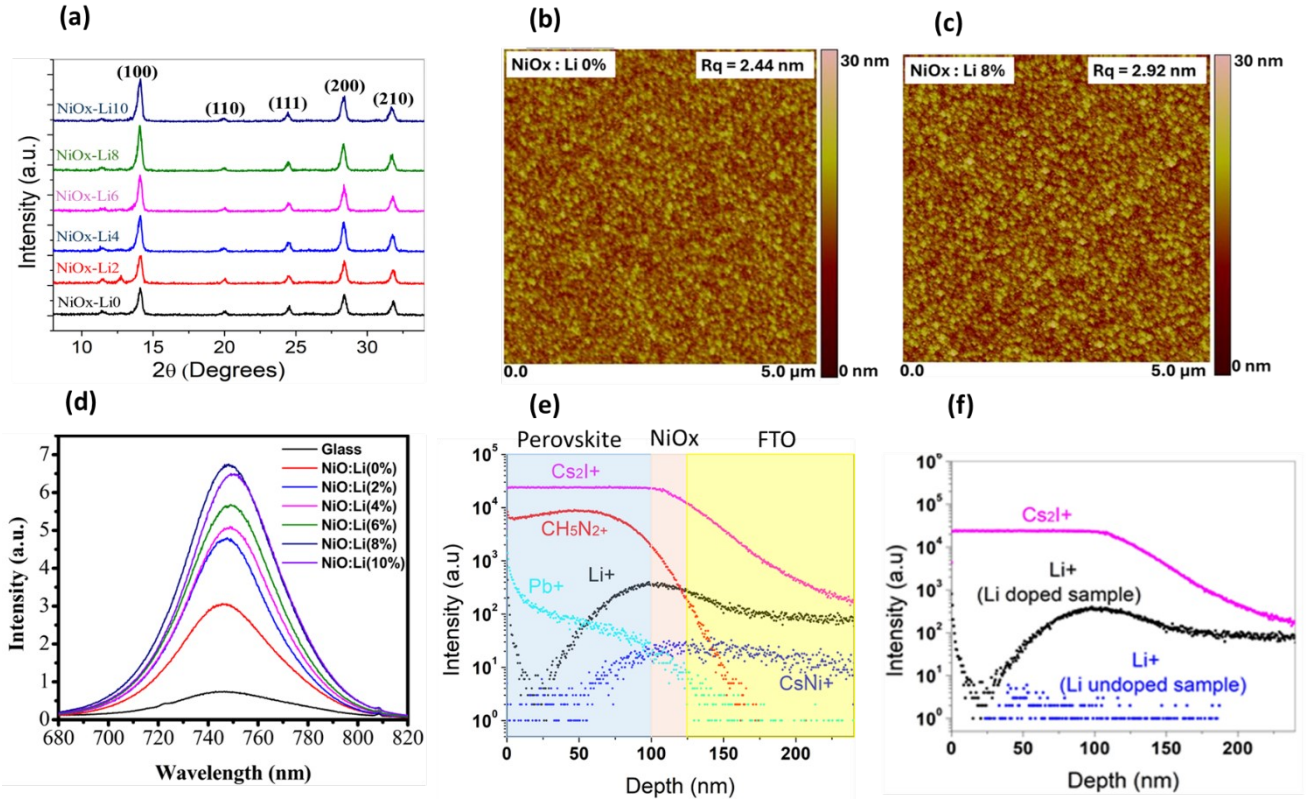

Figure 2 (a) XRD pattern of perovskite films deposited on different Li-doped NiOx films, (b) AFM image for Li-0% NiOx (c) AFM image for Li-8% NiOx (d) Steady state PL intensity of perovskite films deposited on different Li-doped NiOx films, (e) TOF SIMS depth profile for device grown on Li-4% NiOx, (f) Comparison of Li concentrations in the TOF SIMS profile for devices grown on Li-4% and Li-0% NiOx films

View Article Online
DOI: 10.1039/D5YA00072F

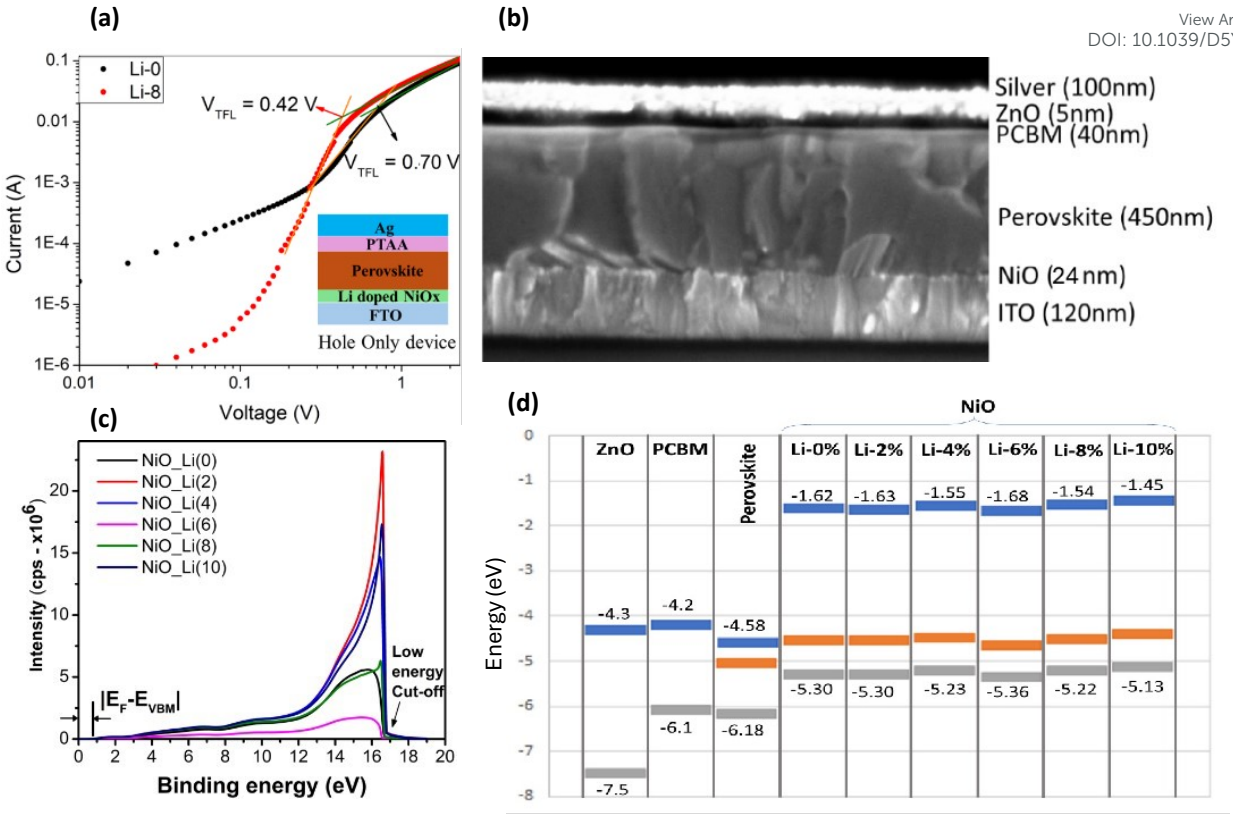

Figure 3 (a) Dark JV curves and V_{TFL} calculation for 0 and 8% Li- doped NiOx hole only devices (Inset: Device structure for hole only devices), (b) Cross sectional SEM image of the perovskite solar cell device, (c) UPS characterization of different Li-doped NiOx HTL, (d) Energy band alignment of perovskite with different Li-doped NiOx HTL

into the diagram.[11,63] The results of UPS analysis did not reveal significant alteration in energy band position. The optical bandgap for all compositions remained essentially unchanged. The position of VBM with respect to the Fermi level also remained nearly unchanged, which is consistent with the observed change in resistivity with Li doping. This suggests that the shift in energy level in the conduction band and valance band position is attributed mainly to the change in the work

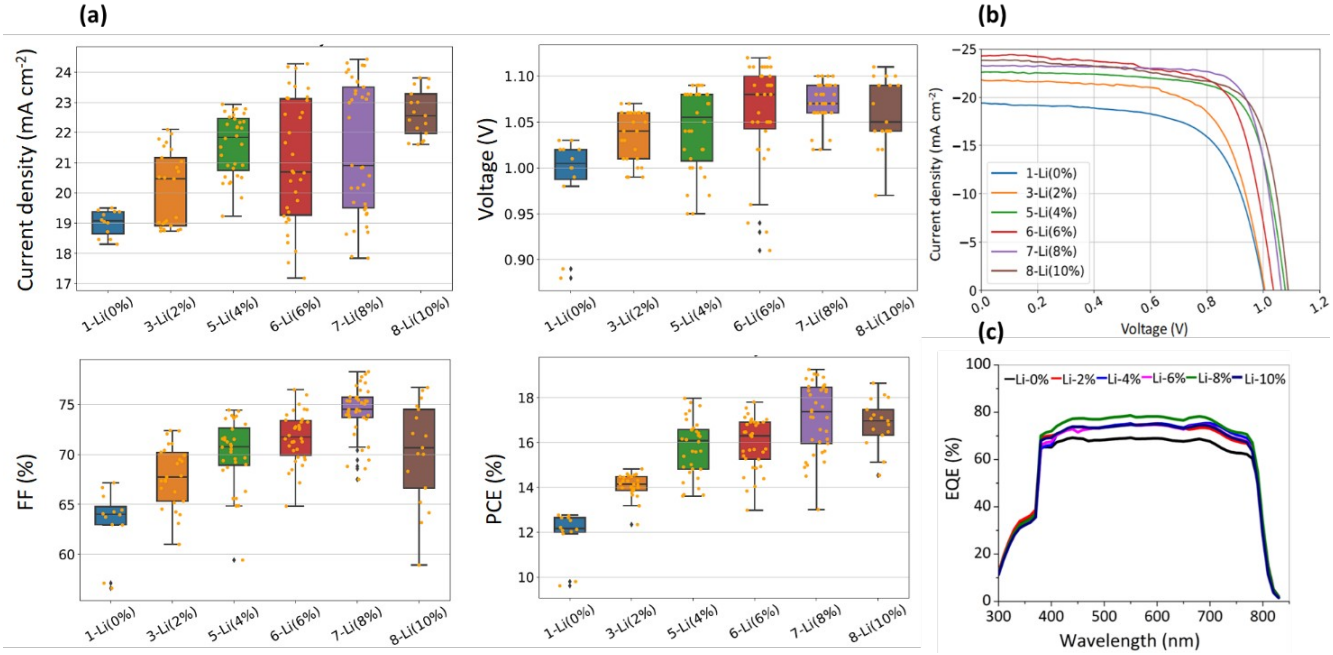

Figure 4 (a) Device performances of PSCs with different Li doped NiOx HTL, (b) J-V curves of best cells for different Li-doped NiOx devices and (c) EQE plot of perovskite solar cells on different Li- doped NiOx HTL.

View Article Online
DOI: 10.1039/D5YA00072F

function of NiO_X. The work function was determined by calculating the difference between the UV energy and the low energy cut-off as shown in Figure 3c. The work function showed a gradual change, from 4.55 eV to 4.42 eV with a slight difference of 0.13 eV, with the increased Li doping (Figure 3d). This change might have some impact on V_{OC} of the devices. However, a direct correlation could not be established.

Performance of the perovskite solar cells: Motivated by the improved crystallinity of perovskite films and passivated nonradiative recombination induced by Li doping, we fabricated the inverted planar solar cell devices using PCBM (40 nm) and ZnO (5 nm) as electron transport layers. Our perovskite formulation is a triple cation CsFAMA (MA: methylammonium, FA: formamidinium and Cs) mixed halide (Cl, Br, and I) perovskite, which is a popular compound that is thermally more stable and enables more reproducible device performances as compared with highly efficient FAMA perovskite.[64] The SEM cross-section image of the complete device is shown in Figure 3b, which depicts a compact perovskite layer along with other layers.

The device performances were compared using a box and whiskers plot, which showed an improvement in all the solar cell parameters with increased Li doping (Figure 4a). The overall device performances with Li doping in the NiOx HTL is summarized in Table 1 and the best JV curves are shown in Figure 4b. The increase in average current density of solar cell devices upon Li doping in the NiOx can be attributed to the improved radiative recombination of the charge carriers in the absorber layer, resulting in higher carrier collection, which led to the boost in the current density. This is further proved by the external quantum efficiency (EQE) plots of the PSC devices based on different lithium doped NiOx (figure 4c), which indicate the improved perovskite absorber quality upon doping the NiOx with lithium.

Table 1 Performance of different Li doped NiOx based perovskite solar cells

Sample	J_{sc} (mA/cm^2)	V_{oc} (V)	Fill Factor (%)	Efficiency (%)
Li-0%	19.00 ± 0.37	0.99 ± 0.05	63.35 ± 3.02	11.47 ± 1.30
Li-2%	20.17 ± 1.22	1.03 ± 0.03	67.83 ± 3.08	14.10 ± 0.52
Li-4%	21.54 ± 1.04	1.04 ± 0.04	70.01 ± 3.34	15.79 ± 1.26
Li-6%	21.05 ± 2.08	1.06 ± 0.06	71.74 ± 2.51	15.98 ± 1.16
Li-8%	21.44 ± 2.17	1.07 ± 0.02	74.18 ± 2.62	17.00 ± 1.57
Li-10%	22.61 ± 1.06	1.06 ±0.03	70.45 ± 5.00	16.70 ± 1.05

Likewise, the enhancement in the open circuit voltage (V_{OC}) could be attributed to the proper energy level alignment of the perovskite valence band with the valence band of Li-doped NiOx resulting in smaller energy offsets. The reduced number of defect sites in the perovskites along with the decrease in the series resistance offered by the Li-doped NiOx resulted in improvement in both the Voc as well as fill factor (FF) of the solar cell devices. These improvements in all the parameters achieved by doping up to 8% Li concentration in NiO_X contributed to the enhanced PCE of the devices. With these aggregate effects, the PCE of the best device increased from approximately 12% without Li doping to a maximum of 19.3% at 8% Li doping, representing a 60.8% improvement.

Conclusions

This research investigated the effect of Li doping on the electrical and optical properties of NiOx hole transport layer. Li doping in NiOx improved the crystallinity and optical properties of subsequent perovskite absorber layer, as confirmed by the results. Furthermore, TOF-SIMS analysis on the perovskite film deposited on lithium doped NiOx revealed the migration of small Li ions from Li-doped NiOx HTL into the perovskite layer. This migration enhanced the device performance by passivating the nonradiative recombination centers and improving the crystallinity of the perovskite material. As a result of these combined effects, the PCE of the best device increased by 60.8%, rising from approximately 12% without Li doping to a peak of 19.3% with 8% Li doping.

Author contributions

Rajbhandari performed the experiment, analyzed the data and wrote the manuscript. Rijal and Chen performed further analysis and edited the manuscript. Choudhary and Efstathiadis performed TOF-SIMS measurement and provided analysis of the depth-profile data. Dhakal conceptualized the idea, secured funding, advised the research, and edited the manuscript.

Conflicts of interest

There are no conflicts to declare.

Data availability

The data generated in this research are available in the Mendeley data repository at https://data.mendeley.com/drafts/t82zfxrhwf

View Article Online
DOI: 10.1039/D5YA00072F

Acknowledgements

This work in part is supported by the National Science Foundation under Grant Number 1751946.

References

(1) Liu, S.; Biju, V. P.; Qi, Y.; Chen, W.; Liu, Z. Recent Progress in the Development of High-Efficiency Inverted Perovskite Solar Cells. *NPG Asia Materials 2023 15:1* **2023**, *15* (1), 1–28. https://doi.org/10.1038/s41427-023-00474-z.

(2) Chen, Z.; Reyes Ramos, W.; Singh Khinda, G.; Amey, J.; Poliks, M. D.; Smilgies, D. M.; Dhakal, T. P. Multipass Inkjet Printing of Lead Halide Perovskite Pixels onto Flexible Substrates. *ACS Applied Optical Materials* **2023**, *1* (9), 1527–1534. https://doi.org/10.1021/ACSAOM.3C00164.

(3) Chen, Z.; Dhakal, T. P. Room Temperature Synthesis of Lead-Free FASnI3perovskite Nanocrystals with Improved Stability by SnF2additive. *Appl Phys Rev* **2023**, *10* (1). https://doi.org/10.1063/5.0125100/19826323/011404_1_ONLINE.PDF.

(4) Meng, L.; You, J.; Guo, T.-F.; Yang, Y. Recent Advances in the Inverted Planar Structure of Perovskite Solar Cells. https://doi.org/10.1021/acs.accounts.5b00404.

(5) Luo, D.; Yang, W.; Wang, Z.; Sadhanala, A.; Hu, Q.; Su, R.; Shivanna, R.; Trindade, G. F.; Watts, J. F.; Xu, Z.; Liu, T.; Chen, K.; Ye, F.; Wu, P.; Zhao, L.; Wu, J.; Tu, Y.; Zhang, Y.; Yang, X.; Zhang, W.; Friend, R. H.; Gong, Q.; Snaith, H. J.; Zhu, R. Enhanced Photovoltage for Inverted Planar Heterojunction Perovskite Solar Cells.

(6) Zhao, L.; Sun, X.; Yao, Q.; Huang, S.; Zhu, L.; Song, J.; Zhao, Y.; Qiang, Y. Field-Effect Control in Hole Transport Layer Composed of Li:NiO/NiO for Highly Efficient Inverted Planar Perovskite Solar Cells. *Adv Mater Interfaces* **2022**, *9* (2), 2101562. https://doi.org/10.1002/ADMI.202101562.

(7) Hyuck Heo, J.; Ji Han, H.; Kim, D.; Kyu Ahn, T.; Hyuk Im, S. Hysteresis-Less Inverted CH 3 NH 3 PbI 3 Planar Perovskite Hybrid Solar Cells with 18.1% Power Conversion Efficiency. *Energy Environ. Sci. Energy Environ. Sci* **1602**, *8* (8), 1602–1608. https://doi.org/10.1039/c5ee00120j.

(8) Wu, C.-G.; Chiang, C.-H.; Tseng, Z.-L.; Nazeeruddin, M. K.; Hagfeldt, A.; Grä, M. High Efficiency Stable Inverted Perovskite Solar Cells without Current Hysteresis. *Energy Environ. Sci. Energy Environ. Sci* **2015**, *8* (8), 2725–2733. https://doi.org/10.1039/c5ee00645g.

(9) Zhiwen Qiu; Haibo Gong; Guanhaojie Zheng; Shuai Yuan; Hailiang Zhang; Xiaomeng Zhu; Huanping Zhou; Bingqiang Cao. Enhanced Physical Properties of Pulsed Laser Deposited NiO Films via Annealing and Lithium Doping for Improving Perovskite Solar Cell Efficiency. *J Mater Chem C Mater* **2017**, *5* (28), 7084–7094. https://doi.org/10.1039/C7TC01224A.

(10) Zhao, K.; Zhao, Y.; Tan, Y.; Hu, K.; Wang, Z.-S. Boosting the Conductivity of the NiOx Layer through Cerium Doping for Efficient Planar Inverted Perovskite Solar Cells. *ACS Appl Energy Mater* **2021**, acsaem.1c01330. https://doi.org/10.1021/ACSAEM.1C01330.

(11) Chen, W.; Wu, Y.; Yue, Y.; Liu, J.; Zhang, W.; Yang, X.; Chen, H.; Bi, E.; Ashraful, I.; Grätzel, M.; Han, L. Efficient and Stable Large-Area Perovskite Solar Cells with Inorganic Charge Extraction Layers. *Science (1979)* **2015**, *350* (6263), 944–948. https://doi.org/10.1126/SCIENCE.AAD1015.

(12) Bashir, A.; Haur, L. J.; Shukla, S.; Gupta, D.; Baikie, T.; Chakraborty, S.; Patidar, R.; Bruno, A.; Mhaisalkar, S.; Akhter, Z. Cu-Doped Nickel Oxide Interface Layer with Nanoscale Thickness for Efficient and Highly Stable Printable Carbon-Based Perovskite Solar Cell. *Solar Energy* **2019**, *182* (February), 225–236. https://doi.org/10.1016/j.solener.2019.02.056.

(13) Hsiao, K. C.; Lee, B. T.; Jao, M. H.; Lin, T. H.; Hou, C. H.; Shyue, J. J.; Wu, M. C.; Su, W. F. Chloride Gradient Render Carrier Extraction of Hole Transport Layer for High Voc and Efficient Inverted Organometal Halide Perovskite Solar Cell. *Chemical Engineering Journal* **2021**, *409*, 128100. https://doi.org/10.1016/J.CEJ.2020.128100.

(14) Nkele, A. C.; Nwanya, A. C.; Shinde, N. M.; Ezugwu, S.; Maaza, M.; Shaikh, J. S.; Ezema, F. I. The Use of Nickel Oxide as a Hole Transport Material in Perovskite Solar Cell Configuration: Achieving a High Performance and Stable Device. *Int J Energy Res* **2020**, *44* (13), 9839–9863. https://doi.org/10.1002/ER.5563.

(15) Yi, A.; Chae, S.; Lee, H.; Lee, S. H.; Kim, D.; Kim, H. J. Synergistic Effect of Codoped Nickel Oxide Hole–Transporting Layers for Highly Efficient Inverted Perovskite Solar Cells. *Solar RRL* **2021**, *5* (9), 2100243. https://doi.org/10.1002/SOLR.202100243.

(16) Zhao, J. J.; Su, X.; Mi, Z.; Zhang, Y.; Hu, Y. J.; Guo, H. J.; Jiao, Y. N.; Zhang, Y. X.; Shi, Y.; Hao, W. Z.; Wu, J. W.; Wang, Y.; Gao, C. F.; Cao, G. Z. Trivalent Ni Oxidation Controlled through Regulating Lithium Content to Minimize Perovskite Interfacial Recombination. *Rare Metals* **2022**, *41* (1), 96–105. https://doi.org/10.1007/S12598-021-01800-6/FIGURES/6.

(17) Saki, Z.; Sveinbjörnsson, K.; Boschloo, G.; Taghavinia, N. The Effect of Lithium Doping in Solution-Processed Nickel Oxide Films for Perovskite Solar Cells. *ChemPhysChem* **2019**, *20* (24), 3322–3327. https://doi.org/10.1002/CPHC.201900856.

(18) Zhao, L.; Sun, X.; Yao, Q.; Huang, S.; Zhu, L.; Song, J.; Zhao, Y.; Qiang, Y. Field-Effect Control in Hole Transport Layer Composed of Li:NiO/NiO for Highly Efficient Inverted Planar Perovskite Solar Cells. *Adv Mater Interfaces* **2022**, *9* (2), 2101562. https://doi.org/10.1002/ADMI.202101562.

(19) Lany, S.; Osorio-Guillén, J.; Zunger, A. Origins of the Doping Asymmetry in Oxides: Hole Doping in NiO versus Electron Doping in ZnO. https://doi.org/10.1103/PhysRevB.75.241203.

(20) Saki, Z.; Sveinbjörnsson, K.; Boschloo, G.; Taghavinia, N. The Effect of Lithium Doping in Solution-Processed Nickel Oxide Films for Perovskite Solar Cells. *ChemPhysChem* **2019**, *20* (24), 3322–3327. https://doi.org/10.1002/CPHC.201900856.

(21) Chen, W.; Liu, F.-Z.; Feng, X.-Y.; Djurišić, A. B.; Chan, W. K.; He, Z.-B. Cesium Doped NiOx as an Efficient Hole Extraction Layer for Inverted Planar Perovskite Solar Cells. *Adv Energy Mater* **2017**, *7* (19), 1700722. https://doi.org/10.1002/AENM.201700722.

(22) Teo, S.; Guo, Z.; Xu, Z.; Zhang, C.; Kamata, Y.; Hayase, S.; Ma, T. The Role of Lanthanum in a Nickel

Oxide-Based Inverted Perovskite Solar Cell for Efficiency and Stability Improvement. *ChemSusChem* **2019**, *12* (2), 518–526. https://doi.org/10.1002/CSSC.201802231.

(23) Zhao, L.; Su, G.; Liu, W.; Cao, L.; Wang, J.; Dong, Z.; Song, M. Optical and Electrochemical Properties of Cu-Doped NiO Films Prepared by Electrochemical Deposition. *Appl Surf Sci* **2011**, *257* (9), 3974–3979. https://doi.org/10.1016/J.APSUSC.2010.11.160.

(24) Wan, X.; Jiang, Y.; Qiu, Z.; Zhang, H.; Zhu, X.; Sikandar, I.; Liu, X.; Chen, X.; Cao, B. Zinc as a New Dopant for NiOx-Based Planar Perovskite Solar Cells with Stable Efficiency near 20%. *ACS Appl Energy Mater* **2018**, *1* (8), 3947–3954. https://doi.org/10.1021/ACSAEM.8B00671/ASSET/IMAGES/LARGE/AE-2018-00671W_0008.JPEG.

(25) Parida, B.; Yoon, S.; Ryu, J.; Hayase, S.; Jeong, S. M.; Kang, D.-W. Boosting the Conversion Efficiency Over 20% in MAPbI 3 Perovskite Planar Solar Cells by Employing a Solution-Processed Aluminum-Doped Nickel Oxide Hole Collector. *Cite This: ACS Appl. Mater. Interfaces* **2020**, *12*. https://doi.org/10.1021/acsami.0c04618.

(26) Xie, Y.; Lu, K.; Duan, J.; Jiang, Y.; Hu, L.; Liu, T.; Zhou, Y.; Hu, B. Enhancing Photovoltaic Performance of Inverted Planar Perovskite Solar Cells by Cobalt-Doped Nickel Oxide Hole Transport Layer. *ACS Appl Mater Interfaces* **2018**, *10* (16), 14153–14159. https://doi.org/10.1021/ACSAMI.8B01683.

(27) Thakur, U. K.; Kumar, P.; Gusarov, S.; Kobryn, A. E.; Riddell, S.; Goswami, A.; Alam, K. M.; Savela, S.; Kar, P.; Thundat, T.; Meldrum, A.; Shankar, K. Consistently High Voc Values in P-i-n Type Perovskite Solar Cells Using Ni3+-Doped NiO Nanomesh as the Hole Transporting Layer. *ACS Appl Mater Interfaces* **2020**, *12* (10), 11467–11478. https://doi.org/10.1021/ACSAMI.9B18197.

(28) Chen, W.; Zhou, Y.; Wang, L.; Wu, Y.; Tu, B.; Yu, B.; Liu, F.; Tam, H.-W.; Wang, G.; Djurišić, A. B.; Huang, L.; He, Z. Molecule-Doped Nickel Oxide: Verified Charge Transfer and Planar Inverted Mixed Cation Perovskite Solar Cell. *Advanced Materials* **2018**, *30* (20), 1800515. https://doi.org/10.1002/ADMA.201800515.

(29) Wu, Y.; Xie, F.; Chen, H.; Yang, X.; Su, H.; Cai, M.; Zhou, Z.; Noda, T.; Han, L. Thermally Stable MAPbI3 Perovskite Solar Cells with Efficiency of 19.19% and Area over 1 Cm2 Achieved by Additive Engineering. *Advanced Materials* **2017**, *29* (28), 1701073. https://doi.org/10.1002/ADMA.201701073.

(30) Gokdemir Choi, F. P.; Moeini Alishah, H.; Gunes, S. Cerium and Zinc Co-Doped Nickel Oxide Hole Transport Layers for Gamma-Butyrolactone Based Ambient Air Fabrication of CH3NH3PbI3 Perovskite Solar Cells. *Appl Surf Sci* **2021**, *563* (May), 150249. https://doi.org/10.1016/j.apsusc.2021.150249.

(31) Kou, D.-X.; Liu, M.-H.; Zhang, P.-P.; Tian, Q.-W.; Wu, S.-X.; Zhou, W.-H.; Zhou, Z.-J. P-Type Li, Cu-Codoped NiOx Hole-Transporting Layer for Efficient Planar Perovskite Solar Cells. *Optics Express, Vol. 24, Issue 22, pp. A1349-A1359* **2016**, *24* (22), A1349–A1359. https://doi.org/10.1364/OE.24.0A1349.

(32) Zhao, J. J.; Su, X.; Mi, Z.; Zhang, Y.; Hu, Y. J.; Guo, H. J.; Jiao, Y. N.; Zhang, Y. X.; Shi, Y.; Hao, W. Z.; Wu, J. W.; Wang, Y.; Gao, C. F.; Cao, G. Z. Trivalent Ni Oxidation Controlled through Regulating Lithium Content to Minimize Perovskite Interfacial Recombination. *Rare Metals* **2022**, *41* (1), 96–105. https://doi.org/10.1007/S12598-021-01800-6/FIGURES/6.

View Article Online
DOI: 10.1039/D5YA00072F

(33) Sta, I.; Jlassi, M.; Hajji, M.; Ezzaouia, H. Structural, Optical and Electrical Properties of Undoped and Li-Doped NiO Thin Films Prepared by Sol–Gel Spin Coating Method. *Thin Solid Films* **2014**, *555*, 131–137. https://doi.org/10.1016/j.tsf.2013.10.137.

(34) Joseph, D. P.; Saravanan, M.; Muthuraaman, B.; Renugambal, P.; Sambasivam, S.; Raja, S. P.; Maruthamuthu, P.; Venkateswaran, C. Spray Deposition and Characterization of Nanostructured Li Doped NiO Thin Films for Application in Dye-Sensitized Solar Cells. *IOP PUBLISHING NANOTECHNOLOGY Nanotechnology* **2008**, *19*, 485707–485710. https://doi.org/10.1088/0957-4484/19/48/485707.

(35) Park, J. H.; Seo, J.; Park, S.; Shin, S. S.; Kim, Y. C.; Jeon, N. J.; Shin, H. W.; Ahn, T. K.; Noh, J. H.; Yoon, S. C.; Hwang, C. S.; Seok, S. Il. Efficient CH<inf>3</Inf>NH<inf>3</Inf>PbI<inf>3</Inf> Perovskite Solar Cells Employing Nanostructured p-Type NiO Electrode Formed by a Pulsed Laser Deposition. *Advanced Materials* **2015**, *27* (27), 4013–4019. https://doi.org/10.1002/adma.201500523.

(36) Jang, W.-L.; Lu, Y.-M.; Hwang, W.-S.; Chen, W.-C. Electrical Properties of Li-Doped NiO Films. *J Eur Ceram Soc* **2010**, *30*, 503–508. https://doi.org/10.1016/j.jeurceramsoc.2009.05.041.

(37) Oswald, S.; Brückner, W. XPS Depth Profile Analysis of Non-Stoichiometric NiO Films. *Surface and Interface Analysis* **2004**, *36* (1), 17–22. https://doi.org/10.1002/sia.1640.

(38) Zhiwen Qiu; Haibo Gong; Guanhaojie Zheng; Shuai Yuan; Hailiang Zhang; Xiaomeng Zhu; Huanping Zhou; Bingqiang Cao. Enhanced Physical Properties of Pulsed Laser Deposited NiO Films via Annealing and Lithium Doping for Improving Perovskite Solar Cell Efficiency. *J Mater Chem C Mater* **2017**, *5* (28), 7084–7094. https://doi.org/10.1039/C7TC01224A.

(39) Di Girolamo, D.; Francesco Di Giacomo, ab; Matteocci, F.; Giacomo Marrani, A.; Dini, D. Progress, Highlights and Perspectives on NiO in Perovskite Photovoltaics. **2020**. https://doi.org/10.1039/d0sc02859b.

(40) Patil, P. S.; Kadam, L. D. Preparation and Characterization of Spray Pyrolyzed Nickel Oxide (NiO) Thin Films. *Appl Surf Sci* **2002**, *199* (1–4), 211–221. https://doi.org/10.1016/S0169-4332(02)00839-5.

(41) Dutta, T.; Gupta, P.; Gupta, A.; Narayan, J. Effect of Li Doping in NiO Thin Films on Its Transparent and Conducting Properties and Its Application in Heteroepitaxial P-n Junctions. *J Appl Phys* **2010**, *108* (8), 083715. https://doi.org/10.1063/1.3499276.

(42) Snaith, H. J.; Abate, A.; Ball, J. M.; Eperon, G. E.; Leijtens, T.; Noel, N. K.; Stranks, S. D.; Tse, J.; Wang, W.; Wojciechowski, K.; Zhang, W. Anomalous Hysteresis in Perovskite Solar Cells. *J. Phys. Chem. Lett* **2014**, *5*. https://doi.org/10.1021/jz500113x.

(43) Wu, C.-G.; Chiang, C.-H.; Tseng, Z.-L.; Nazeeruddin, M. K.; Hagfeldt, A.; Grä, M. High Efficiency Stable Inverted Perovskite Solar Cells without Current Hysteresis. *Energy Environ. Sci. Energy Environ. Sci* **2015**, *8* (8), 2725–2733. https://doi.org/10.1039/c5ee00645g.

(44) Dawson, J. A.; Naylor, A. J.; Eames, C.; Roberts, M.; Zhang, W.; Snaith, H. J.; Bruce, P. G.; Saiful Islam, M. Mechanisms of Lithium Intercalation and Conversion Processes in Organic−Inorganic Halide Perovskites. **2017**. https://doi.org/10.1021/acsenergylett.7b00437.

(45) Xiao, Z.; Yuan, Y.; Shao, Y.; Wang, Q.; Dong, Q.; Bi, C.; Sharma, P.; Gruverman, A.; Huang, J. Giant Switchable Photovoltaic Effect in Organometal Trihalide Perovskite Devices. *Nat Mater* **2015**, *14* (2), 193–197. https://doi.org/10.1038/nmat4150.

(46) Yoo, E. J.; Lyu, M.; Yun, J. H.; Kang, C. J.; Choi, Y. J.; Wang, L. Resistive Switching Behavior in Organic-Inorganic Hybrid CH3NH3PbI3-XClx Perovskite for Resistive Random Access Memory Devices. *Advanced Materials* **2015**, *27* (40), 6170–6175. https://doi.org/10.1002/adma.201502889.

(47) Nie, W.; Tsai, H.; Blancon, J.-C.; Liu, F.; Stoumpos, C. C.; Traore, B.; Kepenekian, M.; Durand, O.; Katan, C.; Tretiak, S.; Crochet, J.; Ajayan, P. M.; Kanatzidis, MercouriG.; Even, J.; Mohite, A. D. Critical Role of Interface and Crystallinity on the Performance and Photostability of Perovskite Solar Cell on Nickel Oxide. *Advanced Materials* **2018**, *30* (5), 1703879. https://doi.org/10.1002/ADMA.201703879.

(48) Li, Z.; Xiao, C.; Yang, Y.; Harvey, S. P.; Kim, D. H.; Christians, J. A.; Yang, M.; Schulz, P.; Nanayakkara, S. U.; Jiang, C. S.; Luther, J. M.; Berry, J. J.; Beard, M. C.; Al-Jassim, M. M.; Zhu, K. Extrinsic Ion Migration in Perovskite Solar Cells. *Energy Environ Sci* **2017**, *10* (5), 1234–1242. https://doi.org/10.1039/c7ee00358g.

(49) Xiao, C.; Zhang, F.; Li, Z.; Harvey, S. P.; Chen, X.; Wang, K.; Jiang, C. S.; Zhu, K.; Al-Jassim, M. Inhomogeneous Doping of Perovskite Materials by Dopants from Hole-Transport Layer. *Matter* **2020**, *2* (1), 261–272. https://doi.org/10.1016/j.matt.2019.10.005.

(50) Rajbhandari, Pravakar P and Dhakal, T. P. Limit of Incorporating Cesium Cations into Formamidinium-Methylammonium Based Mixed Halide Perovskite Solar Cells. *Nanotechnology* **2020**, *31* (13), 135406. https://doi.org/10.1088/1361-6528/AB6230.

(51) Rajbhandari, P. P.; Dhakal, T. P. Low Temperature ALD Growth Optimization of ZnO, TiO 2 , and Al 2 O 3 to Be Used as a Buffer Layer in Perovskite Solar Cells . *Journal of Vacuum Science & Technology A* **2020**, *38* (3), 032406. https://doi.org/10.1116/1.5139247.

(52) Rajbhandari, P. P.; Dhakal, T. P. Limit of Incorporating Cesium Cations into Formamidinium-Methylammonium Based Mixed Halide Perovskite Solar Cells. *Nanotechnology* **2020**, *31* (13). https://doi.org/10.1088/1361-6528/AB6230.

(53) Saki, Z.; Sveinbjörnsson, K.; Boschloo, G.; Taghavinia, N. The Effect of Lithium Doping in Solution-Processed Nickel Oxide Films for Perovskite Solar Cells. *ChemPhysChem* **2019**, *20* (24), 3322–3327. https://doi.org/10.1002/CPHC.201900856.

(54) Kim, K. H.; Takahashi, C.; Abe, Y.; Kawamura, M. Effects of Cu Doping on Nickel Oxide Thin Film Prepared by Sol–Gel Solution Process. *Optik (Stuttg)* **2014**, *125* (12), 2899–2901. https://doi.org/10.1016/J.IJLEO.2013.11.074.

(55) Zheng, G.; Zhu, C.; Ma, J.; Zhang, X.; Tang, G.; Li, R.; Chen, Y.; Li, L.; Hu, J.; Hong, J.; Chen, Q.; Gao, X.; Zhou, H. Manipulation of Facet Orientation in Hybrid Perovskite Polycrystalline Films by Cation Cascade. *Nature Communications 2018 9:1* **2018**, *9* (1), 1–11. https://doi.org/10.1038/s41467-018-05076-w.

(56) Grosfils, P.; Lutsko, J. F. Impact of Surface Roughness on Crystal Nucleation. *Crystals 2021, Vol. 11, Page 4* **2020**, *11* (1), 4. https://doi.org/10.3390/CRYST11010004.

(57) Fang, Z.; He, H.; Gan, L.; Li, J.; Ye, Z. Understanding the Role of Lithium Doping in Reducing Nonradiative Loss in Lead Halide Perovskites. *Advanced Science* **2018**, *5* (12), 1–6. https://doi.org/10.1002/advs.201800736.

(58) Xie, A.; Hettiarachchi, C.; Maddalena, F.; Witkowski, M. E.; Makowski, M.; Drozdowski, W.; Arramel, A.; Wee, A. T. S.; Springham, S. V.; Vuong, P. Q.; Kim, H. J.; Dujardin, C.; Coquet, P.; Birowosuto, M. D.; Dang, C. Lithium-Doped Two-Dimensional Perovskite Scintillator for Wide-Range Radiation Detection. *Communications Materials 2020 1:1* **2020**, *1* (1), 1–10. https://doi.org/10.1038/s43246-020-0038-x.

(59) Xia, H.; Sun, W.; communications, L. P.-C.; 2015, undefined. Hydrothermal Synthesis of Organometal Halide Perovskites for Li-Ion Batteries. *pubs.rsc.orgHR Xia, WT Sun, LM PengChemical communications, 2015•pubs.rsc.org*.

(60) Li, Z.; Xiao, C.; Yang, Y.; Harvey, S.; … D. K.-… & E.; 2017, undefined. Extrinsic Ion Migration in Perovskite Solar Cells. *pubs.rsc.orgZ Li, C Xiao, Y Yang, SP Harvey, DH Kim, JA Christians, M Yang, P Schulz, SU NanayakkaraEnergy & Environmental Science, 2017•pubs.rsc.org*.

(61) Xiao, C.; Zhang, F.; Li, Z.; Harvey, S. P.; Chen, X.; Wang, K.; Jiang, C. S.; Zhu, K.; Al-Jassim, M. Inhomogeneous Doping of Perovskite Materials by Dopants from Hole-Transport Layer. *Matter* **2020**, *2* (1), 261–272. https://doi.org/10.1016/J.MATT.2019.10.005.

(62) Le Corre, V. M.; Duijnstee, E. A.; El Tambouli, O.; Ball, J. M.; Snaith, H. J.; Lim, J.; Koster, L. J. A. Revealing Charge Carrier Mobility and Defect Densities in Metal Halide Perovskites via Space-Charge-Limited Current Measurements. *ACS Energy Lett* **2021**, *6* (3), 1087–1094. https://doi.org/10.1021/ACSENERGYLETT.0C02599/ASSET/IMAGES/MEDIUM/NZ0C02599_M005.GIF.

(63) Chatterjee, S.; Pal, A. J. Introducing Cu 2 O Thin Films as a Hole-Transport Layer in Efficient Planar Perovskite Solar Cell Structures. https://doi.org/10.1021/acs.jpcc.5b11540.

(64) Saliba, M.; Matsui, T.; Seo, J. Y.; Domanski, K.; Correa-Baena, J. P.; Nazeeruddin, M. K.; Zakeeruddin, S. M.; Tress, W.; Abate, A.; Hagfeldt, A.; Grätzel, M. Cesium-Containing Triple Cation Perovskite Solar Cells: Improved Stability, Reproducibility and High Efficiency. *Energy Environ Sci* **2016**, *9* (6), 1989–1997. https://doi.org/10.1039/C5EE03874J.

View Article Online
DOI: 10.1039/D5YA00072F

Data availability

The data in the paper are available from the Mendeley data repository at https://data.mendeley.com/drafts/t82zfxrhwf